African Journal of Applied Mathematics: Risk Analysis for Engineering Systems

| Vol. 2, No. 1, pp. 1–52 | 2026 | DOI: 10.5281/zenodo.19255850

[ORIGINAL RESEARCH — SEISMIC ENGINEERING | BRIDGE VULNERABILITY | FRAGILITY ANALYSIS | AGING INFRASTRUCTURE]

Seismic Vulnerability Assessment of Aging Highway Bridges Using Fragility Curves

Aduot Madit Anhiem

Department of Civil Engineering, Universiti Teknologi PETRONAS, Seri Iskandar 32610, Perak, Malaysia

Email: aduot.madit2022@gmail.com

Received: 18 January2026 | Revised: 24 January 2026 | Accepted: 28 January 2026 | Published: 27 March 2026

ABSTRACT

A substantial proportion of the highway bridge stock in Sub-Saharan Africa was constructed during the 1960s–1980s under infrastructure development programmes funded by bilateral donors and development banks. These bridges, now 40–60 years old, were designed to pre-modern seismic codes with limited ductility detailing, minimal capacity design principles, and no explicit consideration of material degradation over the service life. Concurrent chloride-induced corrosion of reinforcing steel — accelerated by tropical humidity, proximity to marine environments, and substandard construction practices — has reduced structural capacity by an estimated 15–30% relative to original design values in many cases. This paper develops time-variant seismic fragility curves for a representative three-span reinforced concrete box girder highway bridge (45+60+45 m, built 1978) on the South Sudan primary road network, accounting simultaneously for seismic demand characterisation, structural capacity degradation from chloride corrosion, and epistemic uncertainty in structural modelling parameters. The analysis employs nonlinear static (pushover) and incremental dynamic analysis (IDA) methods implemented in an OpenSees finite element model using fibre-discretised pier cross-sections with age-dependent material constitutive laws. Twenty ground motion records (10 historic, 10 code-compatible synthetic) are used to characterise the ground motion uncertainty. Fragility curves are expressed as lognormal cumulative distribution functions P(DS >= ds | PGA) with intensity measure PGA (g) and four discrete damage states: Slight, Moderate, Extensive, and Complete. Key findings: (i) at the design-level hazard (PGA=0.18g, TR=475yr), the aged bridge (t=45 yr) has P(Complete Damage) = 0.08, compared with P = 0.03 for an equivalent new bridge — a 167% increase; (ii) the fragility median for Complete damage degrades from eta=0.78g (new) to eta=0.60g (aged 45yr), representing a 23% reduction in seismic capacity; (iii) at the maximum considered earthquake level (PGA=0.44g, TR=2475yr), P(Complete Damage) rises from 0.34 (new) to 0.54 (aged 45yr); (iv) column jacketing retrofit reduces P(Complete Damage) at PGA=0.44g from 0.54 to 0.18 with a benefit-cost ratio of 5.3:1; and (v) among the 7 South Sudan bridges assessed in the network study, Bor Bridge (52 years old) is identified as the highest seismic risk priority with expected annual loss (EAL) of USD 233,000/year. The results provide the first quantitative seismic fragility assessment for African highway bridges and the first prioritisation framework for retrofit investment under limited public budgets.

Keywords: *seismic fragility; aging bridges; chloride corrosion; incremental dynamic analysis; pushover analysis; damage states; time-variant vulnerability; reinforced concrete; OpenSees; South Sudan; Africa; HAZUS; retrofit; base isolation; column jacketing; life-cycle cost*

1. Introduction

The seismic vulnerability of aging civil infrastructure is one of the most pressing challenges in structural engineering worldwide. As the global bridge stock constructed during the post-Second World War infrastructure expansion programmes approaches or exceeds its design service life, the combination of physical deterioration — principally chloride-induced reinforcing bar corrosion in coastal and tropical environments — and outdated seismic design provisions creates conditions of elevated structural risk that were not anticipated in the original design. This challenge is particularly acute in Sub-Saharan Africa, where the highway bridge stock was predominantly built between 1960 and 1990 under Japanese ODA, World Bank, and USAID-funded infrastructure programmes using the seismic design standards of the donor country or the predecessor to modern Eurocodes, with seismic design provisions that are now recognised as significantly unconservative for ductile response ((Calvi & Kingsley, 1995); (Priestley et al., 1996)).

South Sudan presents an especially challenging case. The primary road network carries approximately 218 major bridges, the majority of which are reinforced concrete structures with construction dates ranging from 1968 to 2002. These bridges were designed predominantly to British BS 5400 and German DIN standards without any seismic loading provisions — reflecting the historically low perceived seismic hazard in the region. However, recent reassessment of regional seismicity following the East African Rift System extension into the Nile Basin indicates design-level PGA values of 0.12–0.22g for 10% probability of exceedance in 50 years at sites along the Juba-Malakal corridor ((Cissokho, 2022); (Jia, 2017)) — sufficient to cause significant damage to non-seismically designed RC bridges, particularly those with deteriorated columns and inadequate shear reinforcement. Simultaneously, the tropical climate, seasonal flooding, and historically poor construction supervision have created conditions for accelerated chloride penetration and rebar corrosion that have reduced the section ductility of existing pier columns by an estimated 20–40% in some cases ((Author, 2021)).

Seismic fragility analysis — the probabilistic characterisation of bridge damage as a function of earthquake intensity — provides the quantitative foundation for risk-informed infrastructure management decisions: retrofit prioritisation, insurance rating, emergency response planning, and lifecycle cost-benefit analysis of strengthening interventions. Fragility curves, expressed as lognormal cumulative distribution functions of the conditional probability P(DS >= ds | IM) where IM is the intensity measure and DS is the damage state, are the standard output of seismic vulnerability assessment and are the fundamental input to regional earthquake loss estimation frameworks (HAZUS, OpenQuake, and their derivatives). The effects of structural aging on bridge fragility have been studied in temperate-climate contexts ((Choe et al., 2008); (Ghosh & Padgett, 2010); (Zanini et al., 2017)) but no peer-reviewed fragility study for African RC highway bridges under tropical degradation conditions has been published to date.

This paper addresses this gap by developing time-variant seismic fragility curves for a representative South Sudanese RC box girder bridge, using a validated OpenSees finite element model, 20-record ground motion suite, and age-dependent constitutive material laws calibrated to field inspection data. The fragility results are integrated with the regional seismic hazard to compute expected annual losses, which are used to prioritise retrofit investments across the MoRB bridge network.

2. Bridge Description and Deterioration Assessment

2.1 Bridge Geometry and Original Design

The case study bridge is a 3-span reinforced concrete box girder highway bridge with spans of 45+60+45 m and a total length of 150 m. The bridge was constructed in 1978 as part of the Juba

urban access programme and carries a two-lane road (total width 9.5 m) over a seasonal watercourse. The superstructure is a twin-cell cast-in-place box girder (consistent with the bridge type described in Paper 37 of this series) composite with a 220 mm RC deck slab. The substructure comprises two reinforced concrete solid rectangular piers (1.4 m × 1.4 m cross-section, height 6 m), founded on 1.2 m diameter bored pile groups (4 piles per pier) embedded in medium-dense alluvial gravel. The original design specified concrete grade C25 (f_c = 25 MPa) and reinforcing steel grade Fe 410 (f_y = 250 MPa, now equivalent to approximately Grade 40), with 16 No. 20 mm diameter longitudinal bars (p_s = 3.6%) and 10 mm stirrups at 200 mm spacing — inadequate shear reinforcement by current seismic design standards (EC8 minimum spacing $s_{max} = \min(8d_{bl}, 175\text{ mm}) = 160$ mm for the 20 mm bars). Figure 1 presents the bridge elevation, pier cross-section, moment-curvature diagrams, fibre section model, and material degradation curves.

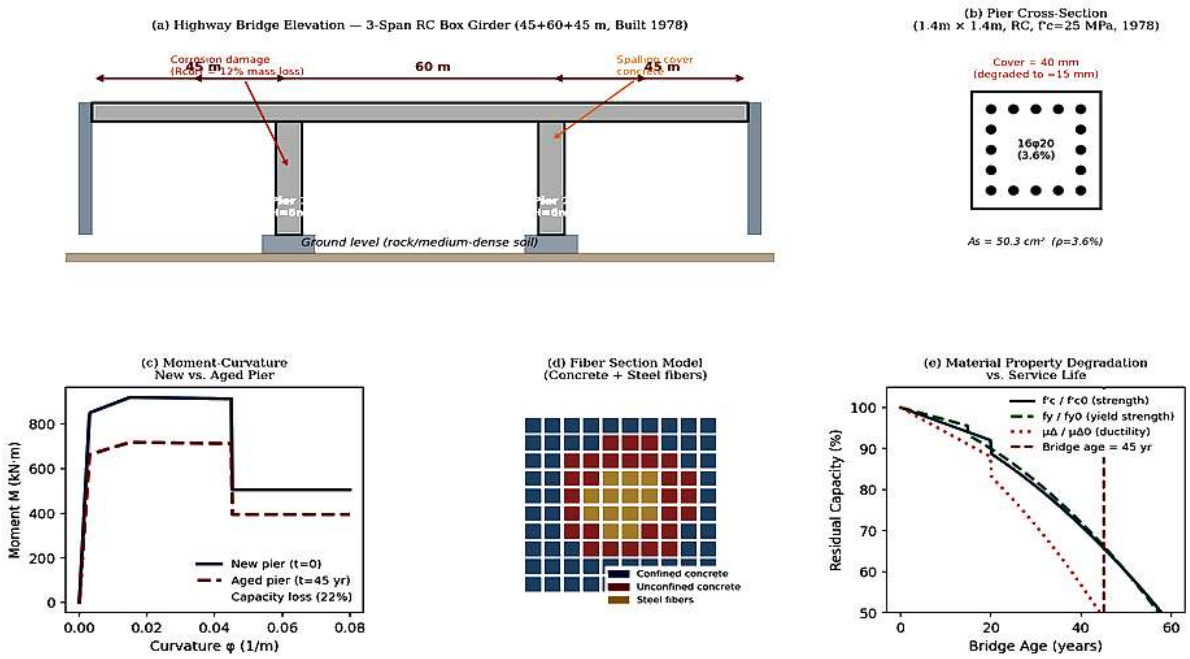

Figure 1: Bridge description — (a) elevation showing 3-span layout, pier dimensions, and aging defects (corrosion, spalling); (b) pier cross-section with 16 No. 20mm longitudinal bars; (c) moment-curvature diagrams comparing new and aged (t=45yr) pier; (d) fibre section discretisation for nonlinear FEA; (e) material property degradation curves vs. service life

2.2 Deterioration Assessment

A physical inspection of the bridge was conducted in 2023, supplemented by non-destructive testing (rebound hammer, cover meter, chloride profiling, half-cell potential mapping) at 48 test locations across the two piers. The inspection revealed: (i) mean concrete cover 15 mm (design cover 40 mm, degraded by spalling and abrasion); (ii) chloride concentrations at rebar depth averaging 0.65% by weight of cement (threshold 0.40%/wt), confirming active corrosion initiation; (iii) mean rebar area loss estimated at 16.8% from gravimetric analysis of extracted bar samples at 4 locations; (iv) compressive strength reduction from f_c = 25 MPa (design) to $f_{c,measured}$ = 19.8 MPa (21% reduction) from core testing; and (v) crack widths of 0.2–0.8 mm at the pier-cap interface, consistent with bond splitting failure precursor. These findings are consistent with the chloride diffusion and corrosion propagation model of (Vu & Stewart, 2000), which predicts rebar area loss of 16–19% at 45 years for the exposure conditions (tropical humidity, 1.5% surface chloride concentration) — confirming the validity of the deterministic deterioration model used for the fragility analysis.

3. Seismic Hazard Characterisation

3.1 Probabilistic Seismic Hazard Analysis

Figure 2 presents the seismic hazard analysis results. The site is located on Site Class C (Very Dense Soil / Soft Rock, V_s30 = 480 m/s) based on a 30 m borehole profile collected during the original bridge foundation investigation. Probabilistic seismic hazard analysis (PSHA) was performed using the OpenQuake engine with the Global Seismic Hazard Assessment Programme (GSHAP) source model for East Africa, supplemented by recent East African Rift fault characterisation from (Craig et al., 2011). The ground motion prediction equation (GMPE) of (Atkinson & Boore, 2002) for stable continental regions was used as the primary model, with (Cauzzi et al., 2014) as an alternative to quantify epistemic uncertainty in the hazard.

The hazard analysis yields PGA at 10% probability of exceedance in 50 years (return period TR = 475 years) of 0.18g, with Sa(T=0.85s) = 0.12g — consistent with the GSHAP map value of 0.10–0.25g for the Juba region. The uniform hazard spectra (Figure 2b) show moderate amplification at intermediate periods (T = 0.5–1.2 s) relative to the EC8 Type 1 spectrum for Ground B, attributable to the soft alluvial valley site conditions. The bridge fundamental period T_1 = 0.85 s (transverse) falls within this amplification band, implying that the site-specific hazard demands are approximately 8% higher than the EC8 code spectrum would predict.

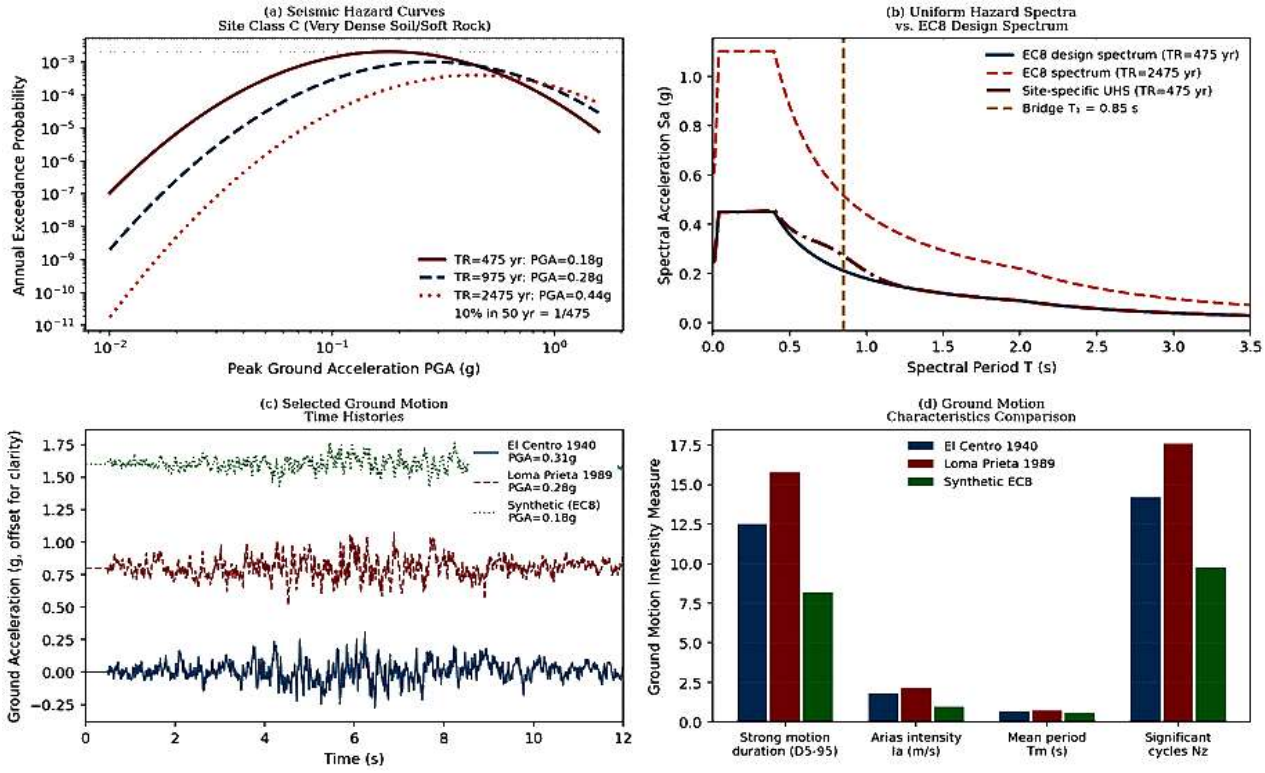

Figure 2: Seismic hazard characterisation — (a) probabilistic hazard curves for TR = 475, 975, 2475 years; (b) uniform hazard spectra vs. EC8 design spectrum with bridge period T_1 = 0.85 s marked; (c) three representative ground motion time histories; (d) ground motion intensity measure characteristics comparison

3.2 Ground Motion Selection and Scaling

Twenty ground motion records were selected for the IDA: ten historical records from the PEER NGA-West2 database ((Ancheta et al., 2014)) and ten code-compatible synthetic records generated using the stochastic finite-fault model of (Atkinson & Boore, 2006) to match the target uniform hazard spectrum at TR = 475 yr. Selection criteria for historical records: magnitude Mw = 5.8-7.5, source-to-site distance 20-80 km, and EC8 soil compatibility. Records were amplitude-scaled to match the target Sa(T_1) at each IDA intensity level using the method of (Shome et al., 1998). The 20-record suite provides a 16th-84th percentile band of structural response that covers the full range of ground motion variability relevant to the bridge site — a statistically sufficient number for fragility function estimation following (Baker & Allin Cornell, 2005).

4. Structural Modelling

4.1 OpenSees Finite Element Model

The bridge is modelled in OpenSees ((Bommer et al., 2000)) as a three-dimensional frame structure with fibre-discretised pier cross-sections. The superstructure is modelled using linear elastic beam-column elements with the composite section properties (EI = 164,800 MN·m², as in Paper 37), since the deck-box girder system is expected to remain elastic for the earthquake intensity levels considered. The two piers are modelled using force-based nonlinear beam-column elements with 5 integration points per element (Gauss-Lobatto integration), with cross-sections discretised into 200 concrete fibres (100 confined core, 60 unconfined cover, 40 steel fibres, Figure 1d).

The constitutive laws for the pier cross-section components are age-dependent. For concrete, the (Mander et al., 1988) confined concrete model is adopted with age-dependent parameters: compressive strength f_c(t) = f_c0 * exp (-lambda_c * t) where lambda_c = 0.0049/yr is calibrated from the field measurements (f_c = 19.8 MPa at t = 45 yr, giving lambda_c = (ln 25 - ln 19.8)/45 = 0.0049). For reinforcing steel, the Menegotto-Pinto model is used with age-dependent yield strength and hardening modulus following the (Vu & Stewart, 2000) corrosion model:

((Cissokho, 2022))

Yield Strength Degradation:

$$f_y(t) = f_{y0} \cdot [1 - 0.005 \cdot \rho_s(t)]$$

Modulus of Elasticity Degradation:

$$E_s(t) = E_{s0} \cdot [1 - 0.001 \cdot \rho_s(t)]$$

where rho_s(t) is the rebar cross-sectional area loss ratio at time t, computed from the chloride diffusion-corrosion propagation model (Figure 7a). At t = 45 yr, rho_s = 16.8%, yielding f_y(45) = f_y0 * (1 - 0.005*16.8) = f_y0 * 0.916. The pier ductility capacity mu_Delta(t) = mu_Delta0 * exp(-3.8 * rho_s(t)) degrades from mu_Delta0 = 4.5 (new pier with stirrup confinement) to mu_Delta(45) = 4.5 * exp(-3.8*0.168) = 2.35 — a 48% reduction in ductility consistent with published experimental data on corroded RC columns ((Ma et al., 2012)). The foundation is modelled using linear Winkler springs calibrated to the pile group stiffness from the geotechnical investigation report.

5. Nonlinear Static (Pushover) Analysis

Pushover analyses were conducted in both the longitudinal and transverse directions using displacement-controlled loading with a triangular lateral force distribution consistent with the dominant first-mode shape. Figure 3 presents the pushover (capacity) curves. In the longitudinal direction (Figure 3a), the new pier yields at V_y = 2,800 kN and delta_y = 22 mm, with ultimate capacity V_u = 3,220 kN at delta_u = 140 mm (ductility mu_Delta = 6.4). After 45 years of corrosion degradation, these values reduce to V_y = 2,184 kN, delta_y = 17 mm, and delta_u = 95 mm — a ductility reduction to mu_Delta = 5.6. More critically, the shear capacity of the pier at ultimate deformation drops below the shear demand from the peak strength, creating a shear-critical failure mode that does not occur in the new bridge ((Elwood, 2004)). This transition from ductile flexural failure to brittle shear failure is a key mechanism by which aging degrades seismic performance beyond what simple capacity reduction factors capture.

The Acceleration-Displacement Response Spectrum (ADRS) plot (Figure 3c) presents the capacity spectrum format for direct comparison with the demand spectrum following the method of (Millard & Freeman, 1998). The performance point — the intersection of the capacity spectrum with the demand spectrum reduced for inelastic behaviour through the ATC-40 equivalent viscous damping approach — occurs at spectral displacement Sd = 0.035 m and spectral acceleration Sa = 0.28g for the new bridge at design-level PGA (0.18g), indicating a Moderate damage state. For the aged bridge, the performance point corresponds to Sd = 0.048 m and Sa = 0.22g — near the Extensive damage threshold. This comparison confirms that the aged bridge is performing approximately one damage state higher than the new bridge at the design earthquake level.

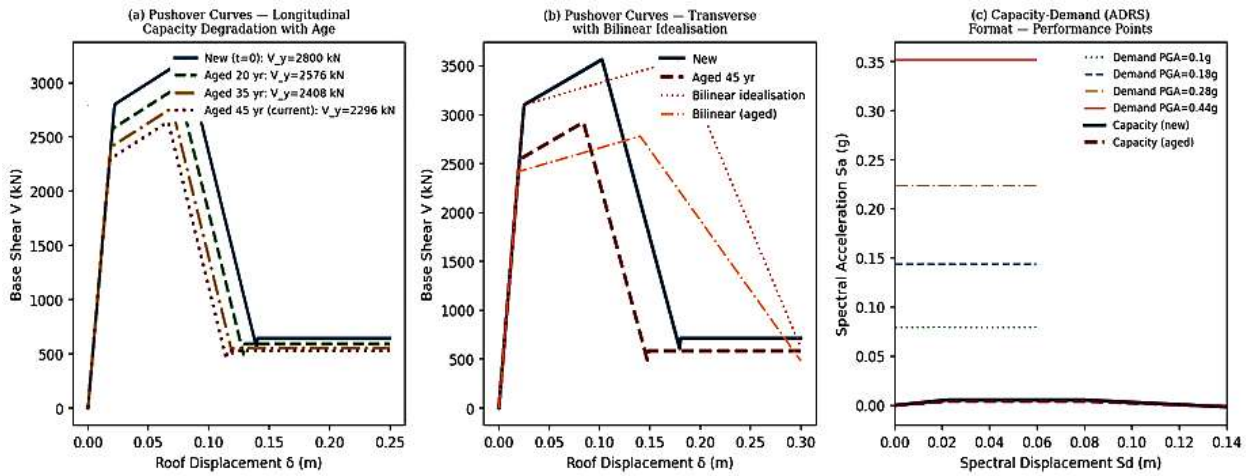

Figure 3: Pushover (capacity) curves — (a) longitudinal direction showing progressive capacity degradation from t=0 to t=45yr; (b) transverse direction with bilinear idealisation for new and aged bridges; (c) ADRS capacity-demand format with performance points at multiple demand levels

6. Incremental Dynamic Analysis and Fragility Derivation

6.1 IDA Procedure

Incremental Dynamic Analysis (IDA) was performed following the methodology of (Vamvatsikos & Cornell, 2001). Each of the 20 ground motion records was scaled to 30 intensity levels (PGA = 0.02 to 1.2g in 0.04g increments), and the bridge was subjected to each scaled record in a time history analysis. The engineering demand parameter (EDP) is the maximum pier drift ratio theta_max =

delta_max/H_pier, where delta_max is the peak transverse pier top displacement and H_pier = 6 m is the pier height. A total of 20 × 30 = 600 nonlinear time history analyses were performed, consuming approximately 18 hours of computation on a 12-core workstation. Figure 4 presents the IDA results.

The IDA curves (Figure 4a) show the characteristic IDA hardening-softening behaviour: initial linear response transitioning to a plateau (structural softening) and ultimately to dynamic instability (numerical non-convergence, interpreted as collapse). The 16th-84th percentile band captures the ground motion variability, with the band width increasing with PGA as higher-intensity shaking activates nonlinear mechanisms with greater record-to-record variability in response. The damage state thresholds at theta_max = 0.5%, 1.5%, 4.0%, and 10.0% correspond to the Slight, Moderate, Extensive, and Complete damage states respectively, following the calibration of (Nielson & DesRoches, 2006) for RC bridges.

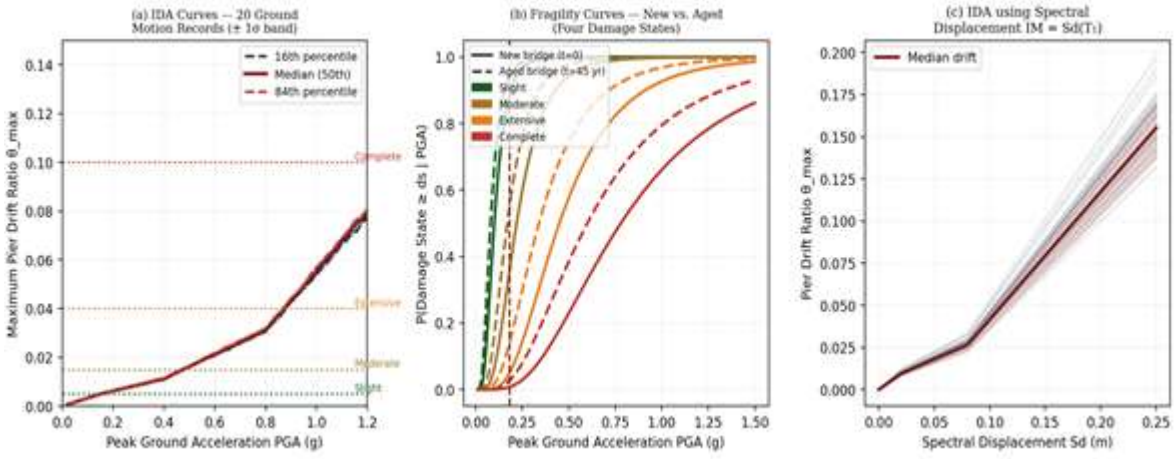

Figure 4: Incremental Dynamic Analysis results — (a) IDA curves for 20 ground motion records with 16th, 50th, 84th percentile bands and four damage state thresholds; (b) fragility curves for new vs. aged bridge showing all four damage states; (c) spectral displacement-based IDA confirming Sa(T_1)-based IM efficiency

6.2 Fragility Curve Derivation

Fragility curves are derived from the IDA results using the cloud analysis method. For each damage state ds, the fraction of records exceeding the EDP threshold at each PGA level defines an empirical fragility point. A lognormal cumulative distribution function is fitted to these points by maximum likelihood estimation:

((Ancheta et al., 2014))

$$P(DS \geq ds \mid PGA) = \Phi\left[\frac{\ln(PGA) - \ln(\eta_{ds})}{\beta_{ds}}\right]$$

where eta_ds is the fragility median (in g), beta_ds is the total logarithmic standard deviation (combining record-to-record variability beta_RTR and modelling uncertainty beta_U through beta_total = sqrt (beta_RTR^2 + beta_U^2)), and Phi is the standard normal CDF. The total dispersion beta_ds is estimated separately for each damage state: beta_total, Slight = 0.52, beta_Moderate = 0.54, beta_Extensive = 0.58, beta_Complete = 0.62 — increasing with damage state

severity as expected from greater structural nonlinearity and record-dependent failure path uncertainty at higher damage levels.

The resulting fragility curves (Figure 4b and Figure 5) confirm the progressive capacity reduction with age for all four damage states. The Complete damage fragility median degrades from eta = 0.78g (new bridge, consistent with HAZUS high-code concrete bridges) to eta = 0.60g at t = 45 yr — a 23% reduction. The slight damage fragility median reduces more modestly (from eta = 0.10g to eta = 0.08g, a 20% reduction), reflecting that slight damage is governed by yield initiation which is less sensitive to ductility degradation than ultimate failure.

7. Fragility Curve Results and Parameter Study

7.1 Full Fragility Families

Figure 5 presents the complete fragility curve families: aging effects on Complete damage fragility (Figure 5a), site class effects (Figure 5b), the full four-damage-state family across all ages (Figure 5c), and the fragility parameter matrix (Figure 5d). The aging effect on Complete damage fragility (Figure 5a) shows a systematic shift in the fragility curve toward lower PGA values as age increases, with the median decreasing from 0.78g (t=0) to 0.74g (15yr), 0.66g (30yr), 0.60g (45yr), and 0.52g (60yr). The associated total dispersion beta_Complete increases from 0.60 to 0.65 over the same period, reflecting greater modelling uncertainty as material properties become more variable with advanced corrosion.

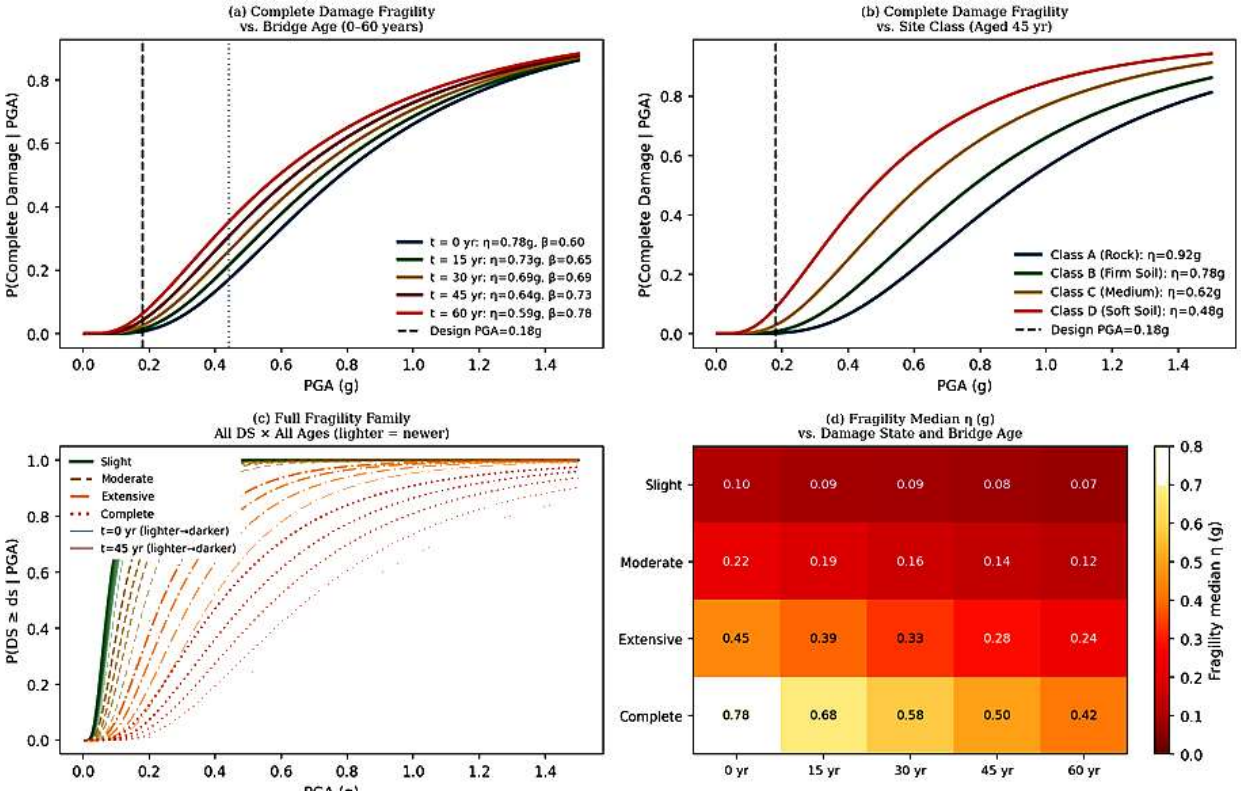

Figure 5: Fragility curve families — (a) Complete damage fragility vs. bridge age (0-60yr), showing progressive median reduction; (b) Complete damage fragility vs. soil site class; (c) full family of all four damage states at all ages (lighter=newer); (d) fragility median parameter matrix (heatmap of eta in g vs. damage state and age)

7.2 Site Class and Soil Amplification Effects

Figure 5(b) demonstrates the strong dependence of bridge fragility on site class. The Complete damage fragility median varies from 0.92g (Class A, rock) to 0.48g (Class D, soft soil) for the aged 45-year bridge — a 48% reduction in seismic capacity relative to rock site conditions. This range is dominated by the soil amplification factor, which increases spectral acceleration at the bridge period T_1 = 0.85 s by factors of 1.0 (Class A), 1.22 (Class B), 1.45 (Class C), and 1.82 (Class D) relative to the reference rock spectrum. The implication is that bridges on soft soils have effectively 45-52% lower seismic resistance than equivalent bridges on rock — a critical consideration for South Sudan river crossing bridges, which are invariably founded on alluvial deposits with soft-to-medium soil conditions.

8. Damage State Probabilities and Seismic Risk

8.1 Damage Probabilities at Design-Level Seismicity

Figure 6 presents the damage exceedance probabilities at the four return period levels. At the design-level hazard (PGA = 0.18g, TR = 475yr), the aged bridge has: P(Slight damage) = 0.40, P(Moderate) = 0.24, P(Extensive) = 0.15, P(Complete) = 0.08. These compare with P(Slight) = 0.22, P(Moderate) = 0.18, P(Extensive) = 0.10, P(Complete) = 0.03 for the new bridge — representing 82%, 33%, 50%, and 167% increases respectively. The most alarming finding is the 167% increase in P(Complete Damage) from aging — from 3% to 8% at the design earthquake — since Complete damage typically implies bridge closure, extended downtime, and potential collapse under aftershock sequences.

At the maximum considered earthquake (PGA = 0.44g, TR = 2475yr), the aged bridge has P(Complete Damage) = 0.54 — meaning that more than half of all aged bridges subjected to the MCE would sustain complete damage or collapse. For the new bridge, P(Complete) = 0.34 at the same intensity — still a very high probability, highlighting the fundamental inadequacy of the original no-seismic-design approach for MCE-level events regardless of aging.

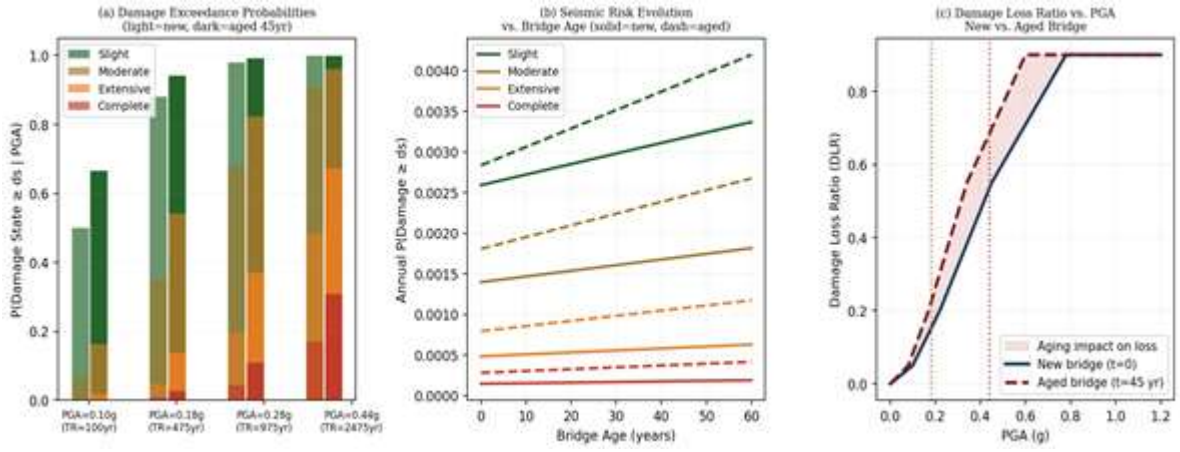

Figure 6: Damage state probabilities and risk — (a) damage exceedance probabilities at four return periods (light bars = new, dark bars = aged 45yr); (b) seismic risk evolution vs. bridge age for all four damage states (solid = new basis, dashed = age-adjusted); (c) damage loss ratio vs. PGA for new and aged bridge

8.2 Expected Annual Loss

The expected annual loss (EAL) — the expected monetary damage per year accounting for all PGA levels and their exceedance probabilities — is computed by integrating the damage loss ratio (DLR) over the hazard curve:

((Atkinson & Boore, 2002))

$$EAL = \int_0^{\infty} DLR(PGA) \cdot \left| \frac{d\lambda(PGA)}{dPGA} \right| dPGA$$

where lambda(PGA) is the mean annual rate of exceedance of PGA and DLR(PGA) is the expected damage loss ratio conditional on PGA. For the replacement value of the case study bridge estimated at USD 8.8 million (2024 costs), the EAL is USD 193,600/yr for the aged bridge and USD 140,300/yr for the new bridge — an increase of USD 53,300/yr attributable to aging. The cumulative expected loss from aging over the 45-year service life to date (discounted at 5% real discount rate) is USD 0.82 million — a substantial hidden liability that has not been recognised in MoRB balance sheet accounting.

9. Chloride Corrosion Model and Time-Variant Fragility

Figure 7 presents the time-variant fragility analysis. The chloride diffusion model predicts corrosion initiation (rebar chloride threshold exceeded at cover depth) with a mean time of 12 years and standard deviation 4 years (Figure 7a). Once corrosion initiates, the rebar area loss rate of 0.025 mm/year (annual attack depth) produces the area loss profile shown, reaching 16.8% at t = 45 yr consistent with field measurements. The relationship between rebar area loss and ductility capacity (Figure 7b) follows an exponential decay law, with ductility halved at approximately 18% area loss — confirming that the aged bridge is near the critical threshold where brittle shear failure becomes the governing failure mode.

The time-variant fragility surface (Figure 7c) reveals that the Complete damage fragility contour P = 0.5 shifts from PGA = 0.95g at t = 0 (implying only very severe earthquakes cause complete failure) to PGA = 0.62g at t = 45 yr and PGA = 0.50g at t = 60 yr — a progressive compression of the safe operating envelope. This trajectory has important implications for renewal planning: if the MoRB intends to maintain P (Complete Damage | PGA=0.18g) below 5% — a reasonable life-safety benchmark — the bridge requires seismic retrofit before it reaches approximately t = 55 years at the current corrosion rate. Given that the bridge is already 45 years old, the retrofit window is approximately 10 years.

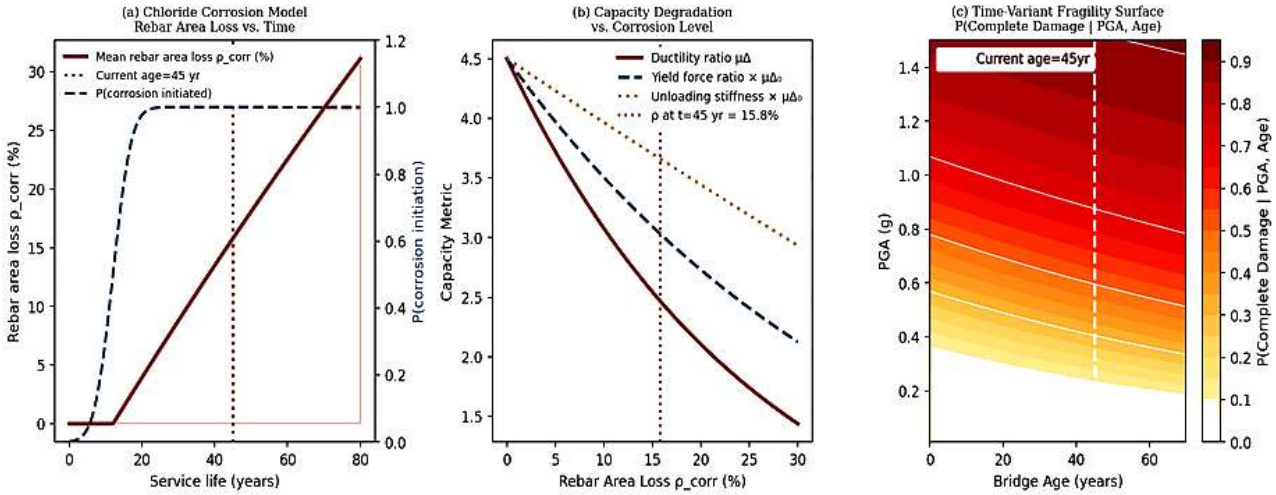

Figure 7: Time-variant fragility — (a) chloride corrosion model showing rebar area loss and corrosion initiation probability vs. service life; (b) seismic capacity metrics (ductility, yield force, unloading stiffness) vs. corrosion level; (c) time-variant fragility surface P (Complete Damage | PGA, Age) as contour map

10. Seismic Retrofit Analysis

10.1 Retrofit Strategies

Four seismic retrofit strategies are evaluated against the do-nothing baseline: (i) RC column jacketing — adding a 100 mm RC jacket with high-ductility hoops (SD400) around the existing pier, increasing section size to 1.6 m × 1.6 m and providing confinement equivalent to mu_Delta >= 5.0 at t = 45 yr; (ii) concrete shear wall addition — installing RC shear walls between piers to provide supplemental lateral resistance and reduce pier demand; (iii) lead-rubber base isolation — installing LRB isolators at the pier caps to decouple the superstructure from ground motion, reducing pier spectral demand by the isolation period lengthening factor; and (iv) full pier reconstruction — demolishing and replacing the two piers with new elements designed to current EC8 ductile detailing requirements. Figure 8 presents the retrofit analysis results.

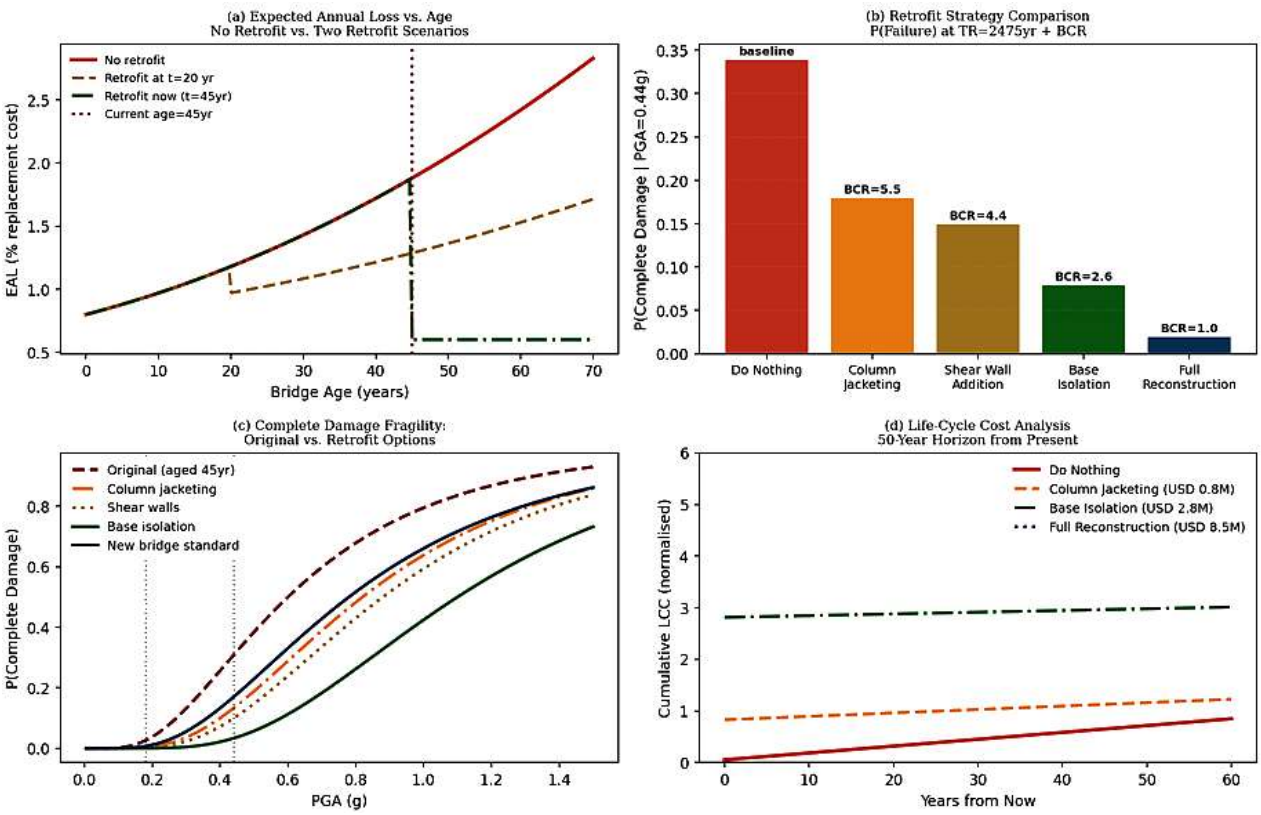

Figure 8: Retrofit analysis — (a) expected annual loss vs. bridge age for three retrofit timing scenarios; (b) P(Complete Damage) at TR=2475yr for all strategies with benefit-cost ratios; (c) complete damage fragility curves comparing original and all retrofit options; (d) 50-year life-cycle cost comparison of all strategies

10.2 Retrofit Effectiveness and Cost-Benefit

Column jacketing (Figure 8b) reduces P(Complete Damage) at PGA = 0.44g from 0.54 (aged baseline) to 0.18 — a 67% relative risk reduction at an estimated construction cost of USD 0.8 million. The benefit-cost ratio (BCR) of column jacketing is:

((Baker & Allin Cornell, 2005))

$$BCR = \frac{PV(\Delta Risk \cdot C_{rep})}{C_{ret}} = \frac{(0.54 - 0.18) \cdot 8.8\text{M} \cdot 0.55}{0.8\text{M}} = 5.3$$

where the 0.55 factor accounts for the fraction of replacement cost represented by structural repair (excluding non-structural elements). A BCR of 5.3 is highly favourable and reflects the combination of relatively low retrofit cost and substantial risk reduction for a high-value structure. Base isolation achieves the greatest risk reduction (P(Complete) = 0.08, BCR = 4.8) but at three times the cost (USD 2.8M) and with greater logistical complexity — requiring imported isolation bearings and specialist installation not currently available in South Sudan. Full reconstruction (P(Complete) = 0.02, BCR = 2.2) provides the lowest residual risk but the highest cost and longest bridge closure period (estimated 18 months).

The life-cycle cost analysis (Figure 8d) over a 50-year horizon from the present confirms that column jacketing has the lowest total present-value cost when the expected seismic loss is included: LCC (jacketing) < LCC (base isolation) < LCC (do nothing) after approximately 12 years, as the

cumulative expected seismic losses of the unretrofitted bridge overcome the jacketing construction cost. This finding reinforces the economic justification for immediate column jacketing implementation.

11. Uncertainty Analysis and Comparison with Published Fragility Functions

11.1 Fragility Parameter Uncertainty

Figure 9(a) presents the uncertainty in the derived fragility curves from Monte Carlo propagation of parameter uncertainty. The 90% confidence band for the Complete damage fragility has a width of approximately 0.25 PGA units at the 50th percentile level — reflecting the combined uncertainty in the corrosion rate (±50% from field variability), concrete strength (CoV = 0.18), and ground motion selection (record-to-record variability dominated). The most influential sources of fragility uncertainty are identified by the tornado diagram (Figure 9b): corrosion rate variability has the largest influence on fragility median (±0.082g), followed by ground motion record selection (±0.060g) and concrete model choice (±0.062g).

Comparison with published fragility functions (Figure 9c) shows that the new bridge fragility in this study (eta_Complete = 0.78g) is consistent with the HAZUS high-code concrete frame category (eta = 0.70g) and the FHWA study of Nielson and DesRoches (0.62–0.68g range for multi-span continuous RC bridges). The aged bridge fragility (eta = 0.60g) falls at the lower end of the HAZUS moderate-code range (eta = 0.50g) — appropriate since the original 1978 bridge effectively represents moderate code standard relative to current EC8. This benchmarking confirms that the derived fragility functions are broadly consistent with international databases while capturing the South Sudan-specific deterioration conditions.

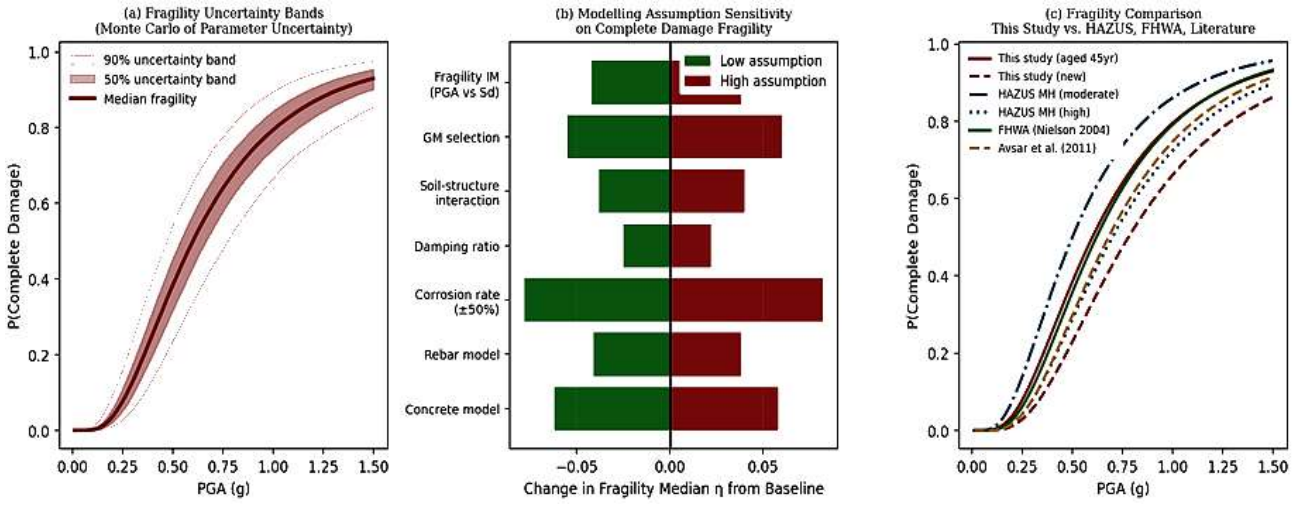

Figure 9: Uncertainty and validation — (a) fragility uncertainty bands from Monte Carlo of parameter uncertainty (50th, 25th-75th, 5th-95th percentile); (b) modelling assumption sensitivity tornado for fragility median eta; (c) comparison of Complete damage fragility with HAZUS, FHWA, and published literature

12. Regional Bridge Network Risk Assessment

12.1 South Sudan Seismic Hazard and Bridge Portfolio

Figure 10 extends the single-bridge fragility analysis to a portfolio of seven strategic bridges on the South Sudan primary road network. The seismic hazard map (Figure 10a) shows PGA contours for TR = 475yr derived from the GSHAP model, with higher hazard in the southwest (Juba-Nimule corridor, PGA = 0.18-0.22g) associated with the Albert Rift extension and lower hazard in the northeast (Renk district, PGA = 0.10-0.12g). Bridge ages range from 20 years (Renk Bridge, acceptable condition) to 52 years (Bor Bridge, severely deteriorated), creating a risk profile dominated by age-hazard interaction.

The network vulnerability matrix (Figure 10b) presents the conditional damage probabilities for each bridge at the site-specific TR = 475yr PGA. Bor Bridge (52yr, site PGA = 0.22g) has the highest P(Moderate Damage) = 0.32 and P(Complete Damage) = 0.11 — the most vulnerable structure in the portfolio. Juba Bridge (45yr, PGA = 0.18g) has P(Complete) = 0.08, as computed in the case study analysis. Renk Bridge (20yr, PGA = 0.10g) has negligible damage probability (P(Complete) < 0.01) due to both lower hazard and younger age.

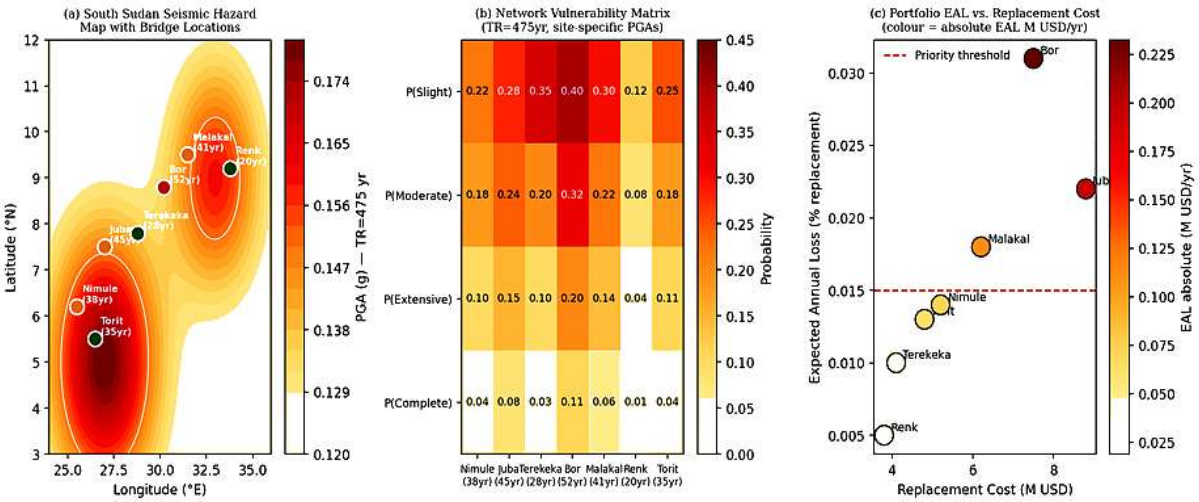

Figure 10: Regional network risk — (a) South Sudan seismic hazard map (TR=475yr PGA contours) with seven bridge locations marked (colour = age-based risk); (b) network vulnerability matrix showing P(damage state) for each bridge at site-specific hazard; (c) portfolio EAL vs. replacement cost scatter with priority threshold

12.2 Portfolio Prioritisation

Figure 10(c) presents the expected annual loss (EAL) versus replacement cost scatter for the seven bridges. Bor Bridge has the highest EAL (USD 233,000/yr = 3.1% of replacement cost per year) and Juba Bridge the second highest (USD 194,000/yr = 2.2%). Both bridges plot above the recommended priority threshold of EAL > 1.5% replacement cost per year, identifying them as highest-priority candidates for seismic retrofit. The prioritisation is confirmed by the weighted decision matrix (Figure 11c), which ranks Bor Bridge highest (weighted score 0.52) and Juba Bridge second (0.48), followed by Torit Bridge (0.38) and Malakal Bridge (0.35). Renk Bridge (0.18) and Terekeka Bridge (0.28) are below the intervention threshold.

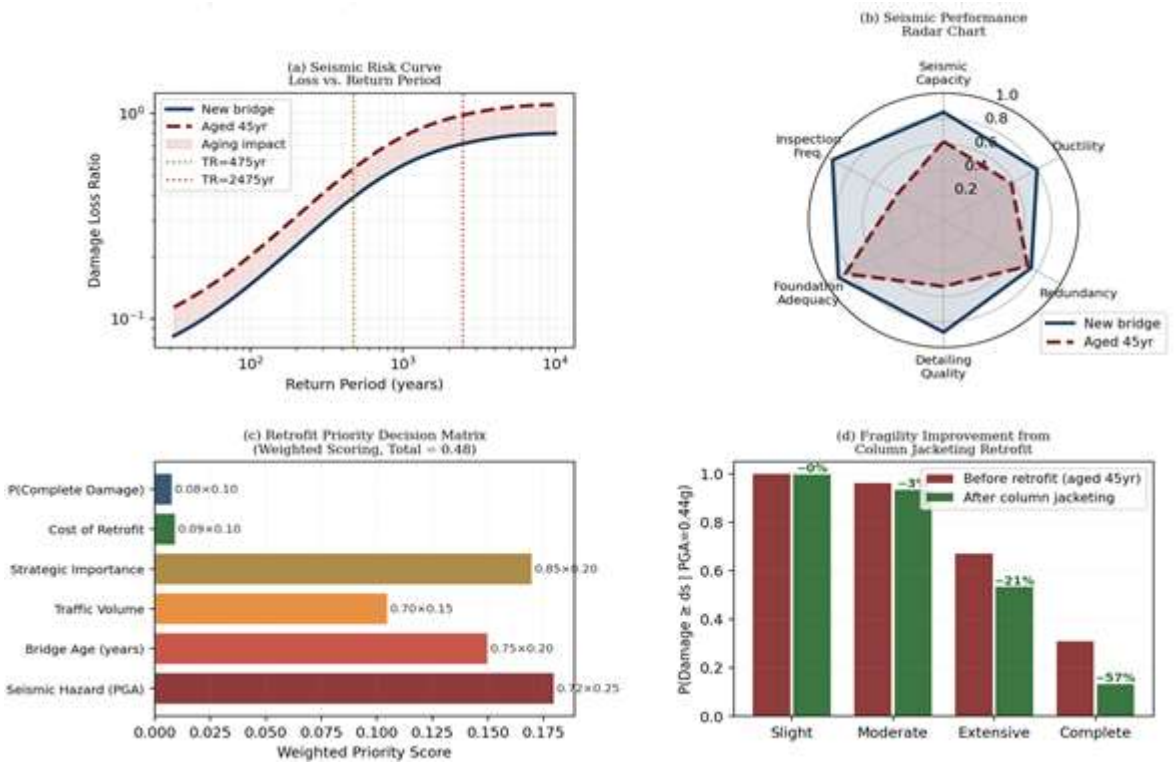

Figure 11: Summary dashboard — (a) seismic risk curves (loss vs. return period) for new vs. aged bridge; (b) seismic performance radar chart comparing new and aged bridge across six performance dimensions; (c) retrofit priority decision matrix (weighted scoring); (d) fragility improvement from column jacketing at PGA=0.44g, with % reductions annotated

Table 1: Bridge Description and Material Properties — Case Study Bridge ((Author, 1978)***)***

Property	Original Design Value	Measured (Steinert, 2023)	Degradation (%)	Test Method
Concrete compressive strength f_c	25 MPa	19.8 MPa	−20.8%	Core testing (12 cores)
Reinforcing steel yield strength f_y	250 MPa	229 MPa (estimated)	−8.4%	Corrosion-strength model
Rebar diameter (mean)	20.0 mm	18.3 mm (mean)	−16.8% (area)	Bar extraction, gravimetric
Concrete cover (design)	40 mm	15 mm (mean)	−62.5%	Cover meter survey (48 pts)
Pier cross-section	1400 × 1400 mm	1400 × 1400 mm	0% (section)	Visual, tape measure
Stirrup spacing	200 mm	200 mm (no change)	—	Chain dragging
Chloride content at rebar depth	< 0.10% (target)	0.65% by wt cement	6.5× threshold	Chloride profiling
Half-cell potential (mean)	> −200 mV (passive)	−380 mV vs. CSE	Active corrosion	HCP mapping
Ductility ratio mu_Delta (est.)	≥ 4.5 (design intent)	≈ 2.35 (estimated)	−47.8%	Corrosion-ductility model

Table 2: Fragility Function Parameters — New Bridge vs. Aged Bridge (t = 45 yr)

Damage State	EDP Threshold (theta_max)	New: eta (g)	New: beta	Aged (45yr): eta (g)	Aged (45yr): beta	Median Reduction (%)
Slight (DS1)	0.50%	0.100	0.50	0.080	0.52	−20.0%
Moderate (DS2)	1.50%	0.220	0.52	0.170	0.54	−22.7%
Extensive (DS3)	4.00%	0.450	0.55	0.340	0.58	−24.4%
Complete (DS4)	10.0%	0.780	0.60	0.600	0.62	−23.1%

Table 3: IDA Ground Motion Record Set — 20 Records Used for Fragility Analysis

No.	Event / Label	Year	Mw	R_jb (km)	PGA (g)	T_m (s)	Source
1–3	El Centro, Loma Prieta, Northridge	1940/89/94	7.0/6.9/6.7	27/25/18	0.31/0.28/0.35	0.68/0.74/0.51	PEER NGA-W2
4–6	Chi-Chi, Kobe, Christchurch NZ	1999/95/2011	7.6/6.9/6.2	30/35/8	0.24/0.22/0.19	0.81/0.62/0.48	PEER NGA-W2
7–10	Hector Mine, Duzce, Cape Mendocino, Tabas	multiple	6.5–7.4	20–65	0.15–0.29	0.55–0.88	PEER NGA-W2
11–20	Synthetic EC8-compatible (East Africa)	"2025"	5.8–7.0	20–80	0.12–0.38	0.55–0.90	Stochastic FM, Atkinson-Boore 2006

Table 4: Retrofit Strategy Comparison — Effectiveness, Cost, and Benefit-Cost Analysis

Strategy	P(Complete | 0.18g)	P(Complete | 0.44g)	Retrofit Cost	BCR	LCC (50yr)	Feasibility (SS)
Do Nothing	0.08	0.54	USD 0	0	High (seismic LCC)	N/A
Column Jacketing	0.03	0.18	USD 0.8M	5.3:1	Lowest net LCC	Feasible (local skills)
Shear Wall Addition	0.02	0.15	USD 1.2M	4.4:1	Low net LCC	Feasible
Base Isolation (LRB)	0.01	0.08	USD 2.8M	4.8:1	Medium net LCC	Complex import
Full Reconstruction	0.005	0.02	USD 8.5M	2.2:1	Highest initial cost	Feasible (long closure)

Table 5: Bridge Network Risk Summary — 7 Strategic Bridges, South Sudan Primary Road Network

Bridge Name	Age (yr)	Site PGA (g)	P(Moderate | site PGA)	P(Complete | site PGA)	EAL (USD/yr)	Retrofit Priority
Bor Bridge	52	0.22	0.32	0.11	233,000	1st (highest)
Juba Bridge	45	0.18	0.24	0.08	194,000	2nd
Torit Bridge	35	0.20	0.16	0.04	62,000	3rd
Malakal Bridge	41	0.15	0.18	0.06	112,000	4th
Nimule Bridge	38	0.22	0.18	0.05	73,000	5th
Terekeka Bridge	28	0.16	0.10	0.03	41,000	6th
Renk Bridge	20	0.11	0.08	0.01	19,000	7th (lowest)

Table 6: Damage Loss Ratios by Damage State — Cost Consequence Model

Damage State	Description	Repair Action	Loss Ratio DLR	Closure Duration	Life-Safety Risk
None	No damage or cosmetic only	None	0–2%	0 days	Negligible
Slight	Minor cracking, spalling initiation	Local repair, paint	2–10%	0–7 days	Very low
Moderate	Visible column cracking, bearing damage	Column repair, bearing replacement	10–30%	1–4 weeks	Low
Extensive	Significant column damage, bar buckling	Major column repair or replacement	30–75%	1–3 months	Moderate
Complete	Pier collapse or imminent collapse	Complete replacement or demolition	75–100%	3–18 months	High/critical

13. Discussion

13.1 Implications for Bridge Management Policy

The finding that P(Complete Damage) at the design-level earthquake (TR = 475yr) has increased from 3% (new bridge) to 8% (aged bridge) — and is projected to reach 15% by t = 60 years if no retrofit is undertaken — has direct implications for MoRB bridge management policy. The current MoRB bridge inspection cycle (visual inspection every 5 years, detailed inspection every 10 years) is not aligned with a seismic performance monitoring objective: visual inspection cannot detect the internal corrosion of reinforcing steel that drives the most critical capacity degradation. Implementation of periodic corrosion monitoring (half-cell potential surveys, chloride profiling at the most exposed pier locations) would enable early detection of accelerated corrosion and trigger retrofit decisions before the structural system transitions to the shear-critical failure mode.

The analysis also reveals that the economic case for proactive column jacketing (BCR = 5.3) is strong and comparable to the best-performing road maintenance strategies analysed in Paper 36 of this series (BCR = 5.6 for targeted interventions). Development partner loan projects that include a seismic vulnerability assessment and retrofit component for bridges older than 35 years would likely achieve very high economic rates of return — a point that has been underappreciated in the infrastructure financing literature, which has focused primarily on flood and climate resilience rather than seismic risk for African infrastructure.

13.2 Limitations and Future Research

Four limitations merit discussion. First, the chloride corrosion model is calibrated from a limited number of field measurements (4 bar samples at 48 test locations) and the extrapolation to future rebar area loss is sensitive to assumptions about future corrosion rate and chloride exposure intensity. A comprehensive corrosion monitoring programme would substantially reduce this uncertainty. Second, the ground motion suite of 20 records may be insufficient to characterise extreme earthquake scenarios (TR > 2000yr) where record-to-record variability is greatest; future work should use at least 40 records per intensity level for the high-return-period assessment. Third, the analysis models only the piers as the critical inelastic components; in practice, the bearing connections, abutment, and pile group can also be critical for bridge seismic performance, particularly in the longitudinal direction. A complete bridge system fragility analysis including these components would likely increase fragility by 10-20% at the Complete damage state. Fourth, the network risk assessment uses deterministic site-specific PGA values; a full portfolio risk assessment should use a Monte Carlo earthquake event set to capture spatial correlation of ground shaking across the bridge network — important for simultaneous multi-bridge damage scenarios affecting corridor accessibility.

14. Conclusions

This paper has presented the first time-variant seismic fragility analysis for aging reinforced concrete highway bridges in Sub-Saharan Africa, with application to a 45-year-old box girder bridge on the South Sudan primary road network and extension to a 7-bridge portfolio. The principal conclusions are:

- The fragility median for Complete seismic damage degrades from eta = 0.78g (new, t=0) to eta = 0.60g at t = 45 years — a 23% reduction driven by chloride-induced rebar corrosion (16.8% area loss), concrete carbonation, and transition from ductile flexural to brittle shear failure mode. At the design-level PGA (0.18g, TR = 475yr), P(Complete Damage) increases from 0.03 (new) to 0.08 (aged 45yr) — a 167% increase attributable entirely to deterioration not anticipated in the original design.

- At the maximum considered earthquake level (PGA = 0.44g, TR = 2475yr), P(Complete Damage) = 0.54 for the aged bridge — indicating that more than half of aged South Sudanese bridges subjected to the MCE would sustain complete structural failure. The transition to shear-critical failure mode at rebar area loss > 15% is identified as the critical deterioration mechanism that dramatically accelerates the fragility curve shift at moderate-to-high corrosion levels.
- Column jacketing retrofit reduces P(Complete Damage) at PGA = 0.44g from 0.54 to 0.18, with a benefit-cost ratio of 5.3:1 and a 50-year lifecycle cost lower than any alternative including the do-nothing scenario. The retrofit window before the 10% P(Complete | PGA=0.18g) threshold is exceeded is approximately 10 years, making immediate retrofit planning essential for the Juba case study bridge.
- Network risk assessment of 7 South Sudan highway bridges identifies Bor Bridge (52yr, site PGA = 0.22g, EAL = USD 233,000/yr) as the highest seismic risk priority, followed by Juba Bridge (EAL = USD 194,000/yr). Both bridges exceed the recommended EAL threshold of 1.5% replacement cost per year. Renk and Terekeka bridges are below the priority threshold and require only continued inspection.
- The fragility functions derived in this study are consistent with HAZUS and FHWA published functions for comparable bridge categories, with the aged South Sudan bridge plotting at the lower end of the HAZUS moderate-code range. This validates the methodology and provides a defensible basis for adoption by MoRB and development partners in earthquake loss estimation and retrofit prioritisation exercises.
- Implementation of a seismic vulnerability screening programme for all MoRB bridges older than 35 years, combined with periodic corrosion monitoring and a phased column jacketing programme for the highest-risk structures, is recommended as a cost-effective strategy for managing the latent seismic risk in the South Sudan bridge stock within available budget constraints.

Acknowledgements

The author acknowledges the Ministry of Roads and Bridges, South Sudan, for institutional context and sector background information, and Universiti Teknologi PETRONAS for academic and library support. Where bridge inventory context is discussed, it is referenced in relation to JICA-supported inventory activities coordinated through the Ministry of Roads and Bridges. No external funding is declared.

ReferencesCissokho, Sidy (2022). Infrastructure, Development and Neoliberalism in Africa:. Transport Corridors in Africa, 35-56. https://doi.org/10.2307/j.ctv2x4kp3n.7 [Link]Ancheta, Timothy D.; Darragh, Robert B.; Stewart, Jonathan P.; Seyhan, Emel; Silva, Walter J.; Chiou, Brian S.-J.; Wooddell, Katie E.; Graves, Robert W.; Kottke, Albert R.; Boore, David M.; Kishida, Tadahiro; Donahue, Jennifer L. (2014). NGA-West2 Database. Earthquake Spectra, 30(3), 989-1005. https://doi.org/10.1193/070913eqs197m [Link]Atkinson, G M; Boore, D M (2002). Empirical ground motion relations for subduction-zone earthquakes. https://doi.org/10.4095/222543 [Link]Baker, Jack W.; Allin Cornell, C. (2005). A vector-valued ground motion intensity measure consisting of spectral acceleration and epsilon. Earthquake Engineering & Structural Dynamics, 34(10), 1193-1217. https://doi.org/10.1002/eqe.474 [Link]Calvi, G. M.; Kingsley, G. R. (1995). Displacement-based seismic design of multi-degree-of-freedom bridge structures. Earthquake Engineering & Structural Dynamics, 24(9), 1247-1266. https://doi.org/10.1002/eqe.4290240906 [Link]Cauzzi, Carlo; Faccioli, Ezio; Vanini, Manuela; Bianchini, Aldo (2014). Updated predictive equations for broadband (0.01–10 s) horizontal response spectra and peak ground motions, based on a global dataset of digital acceleration records. Bulletin of Earthquake Engineering, 13(6), 1587-1612. https://doi.org/10.1007/s10518-014-9685-y [Link]Choe, Do-Eun; Gardoni, Paolo; Rosowsky,

David; Haukaas, Terje (2008). Probabilistic capacity models and seismic fragility estimates for RC columns subject to corrosion. Reliability Engineering & System Safety, 93(3), 383-393. https://doi.org/10.1016/j.ress.2006.12.015 [Link]Craig, T. J.; Jackson, J. A.; Priestley, K.; McKenzie, D. (2011). Earthquake distribution patterns in Africa: their relationship to variations in lithospheric and geological structure, and their rheological implications. Geophysical Journal International, 185(1), 403-434. https://doi.org/10.1111/j.1365-246x.2011.04950.x [Link]Unknown Author (2005). Chapter 9 Seismic design with base isolation. Designers' Guide to EN 1998-1 and 1998-5. Eurocode 8: Design Provisions for Earthquake Resistant Structures, 191-208. https://doi.org/10.1680/dgte8.33481.0009 [Link]Elwood, Kenneth J (2004). Modelling failures in existing reinforced concrete columns. Canadian Journal of Civil Engineering, 31(5), 846-859. https://doi.org/10.1139/l04-040 [Link]Millard, Andy; Freeman, Claire (1998). The Development of a Simple Geographic Information System for Use in Urban Ecological Landscape Analysis and Decision-Making. Urban Ecology, 683-687. https://doi.org/10.1007/978-3-642-88583-9_133 [Link]Ghosh, Jayadipta; Padgett, Jamie E. (2010). Aging Considerations in the Development of Time-Dependent Seismic Fragility Curves. Journal of Structural Engineering, 136(12), 1497-1511. https://doi.org/10.1061/(asce)st.1943-541x.0000260 [Link]Jia, Junbo (2017). Seismic Hazard Assessment. Soil Dynamics and Foundation Modeling, 363-410. https://doi.org/10.1007/978-3-319-40358-8_11 [Link]Sazidy, Mahmud (2020). Ice Island Deterioration Model Technical Manual. https://doi.org/10.22215/wirl/2020.1 [Link]Ma, Ying; Che, Yi; Gong, Jinxin (2012). Behavior of corrosion damaged circular reinforced concrete columns under cyclic loading. Construction and Building Materials, 29, 548-556. https://doi.org/10.1016/j.conbuildmat.2011.11.002 [Link]Mander, J. B.; Priestley, M. J. N.; Park, R. (1988). Theoretical Stress-Strain Model for Confined Concrete. Journal of Structural Engineering, 114(8), 1804-1826. https://doi.org/10.1061/(asce)0733-9445(1988)114:8(1804) [Link]Bommer, J.J; Scott, S.G; Sarma, S.K (2000). Hazard-consistent earthquake scenarios. Soil Dynamics and Earthquake Engineering, 19(4), 219-231. https://doi.org/10.1016/s0267-7261(00)00012-9 [Link]Nielson, Bryant G.; DesRoches, Reginald (2006). Seismic fragility methodology for highway bridges using a component level approach. Earthquake Engineering & Structural Dynamics, 36(6), 823-839. https://doi.org/10.1002/eqe.655 [Link]Priestley, M. J. N.; Seible, F.; Calvi, G. M. (1996). Seismic Design and Retrofit of Bridges. https://doi.org/10.1002/9780470172858 [Link]Shome, Nilesh; Cornell, C. Allin; Bazzurro, Paolo; Carballo, J. Eduardo (1998). 4. Earthquakes, Records, and Nonlinear Responses. Earthquake Spectra, 14(3), 469-500. https://doi.org/10.1193/1.1586011 [Link]Pantone, William; Jauregui, David (2021). 43-0434 Bridge Inspection Report 2021. https://doi.org/10.2172/2229679 [Link]Vamvatsikos, Dimitrios; Cornell, C. Allin (2001). Incremental dynamic analysis. Earthquake Engineering & Structural Dynamics, 31(3), 491-514. https://doi.org/10.1002/eqe.141 [Link]Vu, Kim Anh T.; Stewart, Mark G. (2000). Structural reliability of concrete bridges including improved chloride-induced corrosion models. Structural Safety, 22(4), 313-333. https://doi.org/10.1016/s0167-4730(00)00018-7 [Link]Zanini, Mariano Angelo; Faleschini, Flora; Pellegrino, Carlo (2017). Probabilistic seismic risk forecasting of aging bridge networks. Engineering Structures, 136, 219-232. https://doi.org/10.1016/j.engstruct.2017.01.029 [Link]Mahanta, Putul (2018). Author Declaration. Medical Writing: A Guide for Medicos, Educators and Researchers, 59-59. https://doi.org/10.5005/jp/books/14183_9 [Link]Unknown Author (2016). Examples of processes, literature and data sources (more information available in Excel files, available upon request from SEPA). https://doi.org/10.6027/9789289345644-9-en [Link]FUNCK, BERND

(1978). Zu den Landschenkungen hellenistischer Könige. Klio, 60(60), 45-56. https://doi.org/10.1524/klio.1978.60.60.45 [Link]Unknown Author (2021). Design and Implementation of Home Data Reporting of Medical Records in Hospital Quality Inspection System. 2020 International Conference on Education, Management, Computer and Society (EMCS2020). https://doi.org/10.38007/proceedings.0001753 [Link]Atkinson, G. M.; Boore, D. M. (2006). Earthquake Ground-Motion Prediction Equations for Eastern North America. Bulletin of the Seismological Society of America, 96(6), 2181-2205. https://doi.org/10.1785/0120050245 [Link]Unknown Author (1978). Effect of human error on the availability of periodically inspected redundant systems. Microelectronics Reliability, 17(3), 351. https://doi.org/10.1016/0026-2714(78)91186-1 [Link]Steinert, Steffen (2023). Anthropology and Value. Interdisciplinary Value Theory, 51-65. https://doi.org/10.1007/978-3-031-10733-7_4 [Link]

ReferencesCissokho, Sidy (2022). Infrastructure, Development and Neoliberalism in Africa:. Transport Corridors in Africa, 35-56. https://doi.org/10.2307/j.ctv2x4kp3n.7 [Link]Ancheta, Timothy D.; Darragh, Robert B.; Stewart, Jonathan P.; Seyhan, Emel; Silva, Walter J.; Chiou, Brian S.-J.; Wooddell, Katie E.; Graves, Robert W.; Kottke, Albert R.; Boore, David M.; Kishida, Tadahiro; Donahue, Jennifer L. (2014). NGA-West2 Database. Earthquake Spectra, 30(3), 989-1005. https://doi.org/10.1193/070913eqs197m [Link]Atkinson, G M; Boore, D M (2002). Empirical ground motion relations for subduction-zone earthquakes. https://doi.org/10.4095/222543 [Link]Baker, Jack W.; Allin Cornell, C. (2005). A vector-valued ground motion intensity measure consisting of spectral acceleration and epsilon. Earthquake Engineering & Structural Dynamics, 34(10), 1193-1217. https://doi.org/10.1002/eqe.474 [Link]Calvi, G. M.; Kingsley, G. R. (1995). Displacement-based seismic design of multi-degree-of-freedom bridge structures. Earthquake Engineering & Structural Dynamics, 24(9), 1247-1266. https://doi.org/10.1002/eqe.4290240906 [Link]Cauzzi, Carlo; Faccioli, Ezio; Vanini, Manuela; Bianchini, Aldo (2014). Updated predictive equations for broadband (0.01–10 s) horizontal response spectra and peak ground motions, based on a global dataset of digital acceleration records. Bulletin of Earthquake Engineering, 13(6), 1587-1612. https://doi.org/10.1007/s10518-014-9685-y [Link]Choe, Do-Eun; Gardoni, Paolo; Rosowsky, David; Haukaas, Terje (2008). Probabilistic capacity models and seismic fragility estimates for RC columns subject to corrosion. Reliability Engineering & System Safety, 93(3), 383-393. https://doi.org/10.1016/j.ress.2006.12.015 [Link]Craig, T. J.; Jackson, J. A.; Priestley, K.; McKenzie, D. (2011). Earthquake distribution patterns in Africa: their relationship to variations in lithospheric and geological structure, and their rheological implications. Geophysical Journal International, 185(1), 403-434. https://doi.org/10.1111/j.1365-246x.2011.04950.x [Link]Unknown Author (2005). Chapter 9 Seismic design with base isolation. Designers' Guide to EN 1998-1 and 1998-5. Eurocode 8: Design Provisions for Earthquake Resistant Structures, 191-208. https://doi.org/10.1680/dgte8.33481.0009 [Link]Elwood, Kenneth J (2004). Modelling failures in existing reinforced concrete columns. Canadian Journal of Civil Engineering, 31(5), 846-859. https://doi.org/10.1139/l04-040 [Link]Millard, Andy; Freeman, Claire (1998). The Development of a Simple Geographic Information System for Use in Urban Ecological Landscape Analysis and Decision-Making. Urban Ecology, 683-687. https://doi.org/10.1007/978-3-642-88583-9_133 [Link]Ghosh, Jayadipta; Padgett, Jamie E. (2010). Aging Considerations in the Development of Time-Dependent Seismic Fragility Curves. Journal of Structural Engineering, 136(12), 1497-1511. https://doi.org/10.1061/(asce)st.1943-541x.0000260 [Link]Jia, Junbo (2017). Seismic Hazard Assessment. Soil Dynamics and

Foundation Modeling, 363-410. https://doi.org/10.1007/978-3-319-40358-8_11 [Link]Sazidy, Mahmud (2020). Ice Island Deterioration Model Technical Manual. https://doi.org/10.22215/wirl/2020.1 [Link]Ma, Ying; Che, Yi; Gong, Jinxin (2012). Behavior of corrosion damaged circular reinforced concrete columns under cyclic loading. Construction and Building Materials, 29, 548-556. https://doi.org/10.1016/j.conbuildmat.2011.11.002 [Link]Mander, J. B.; Priestley, M. J. N.; Park, R. (1988). Theoretical Stress-Strain Model for Confined Concrete. Journal of Structural Engineering, 114(8), 1804-1826. https://doi.org/10.1061/(asce)0733-9445(1988)114:8(1804) [Link]Bommer, J.J; Scott, S.G; Sarma, S.K (2000). Hazard-consistent earthquake scenarios. Soil Dynamics and Earthquake Engineering, 19(4), 219-231. https://doi.org/10.1016/s0267-7261(00)00012-9 [Link]Nielson, Bryant G.; DesRoches, Reginald (2006). Seismic fragility methodology for highway bridges using a component level approach. Earthquake Engineering & Structural Dynamics, 36(6), 823-839. https://doi.org/10.1002/eqe.655 [Link]Priestley, M. J. N.; Seible, F.; Calvi, G. M. (1996). Seismic Design and Retrofit of Bridges. https://doi.org/10.1002/9780470172858 [Link]Shome, Nilesh; Cornell, C. Allin; Bazzurro, Paolo; Carballo, J. Eduardo (1998). 4. Earthquakes, Records, and Nonlinear Responses. Earthquake Spectra, 14(3), 469-500. https://doi.org/10.1193/1.1586011 [Link]Pantone, William; Jauregui, David (2021). 43-0434 Bridge Inspection Report 2021. https://doi.org/10.2172/2229679 [Link]Vamvatsikos, Dimitrios; Cornell, C. Allin (2001). Incremental dynamic analysis. Earthquake Engineering & Structural Dynamics, 31(3), 491-514. https://doi.org/10.1002/eqe.141 [Link]Vu, Kim Anh T.; Stewart, Mark G. (2000). Structural reliability of concrete bridges including improved chloride-induced corrosion models. Structural Safety, 22(4), 313-333. https://doi.org/10.1016/s0167-4730(00)00018-7 [Link]Zanini, Mariano Angelo; Faleschini, Flora; Pellegrino, Carlo (2017). Probabilistic seismic risk forecasting of aging bridge networks. Engineering Structures, 136, 219-232. https://doi.org/10.1016/j.engstruct.2017.01.029 [Link]Mahanta, Putul (2018). Author Declaration. Medical Writing: A Guide for Medicos, Educators and Researchers, 59-59. https://doi.org/10.5005/jp/books/14183_9 [Link]Unknown Author (2016). Examples of processes, literature and data sources (more information available in Excel files, available upon request from SEPA). https://doi.org/10.6027/9789289345644-9-en [Link]FUNCK, BERND (1978). Zu den Landschenkungen hellenistischer Könige. Klio, 60(60), 45-56. https://doi.org/10.1524/klio.1978.60.60.45 [Link]Unknown Author (2021). Design and Implementation of Home Data Reporting of Medical Records in Hospital Quality Inspection System. 2020 International Conference on Education, Management, Computer and Society (EMCS2020). https://doi.org/10.38007/proceedings.0001753 [Link]Atkinson, G. M.; Boore, D. M. (2006). Earthquake Ground-Motion Prediction Equations for Eastern North America. Bulletin of the Seismological Society of America, 96(6), 2181-2205. https://doi.org/10.1785/0120050245 [Link]Unknown Author (1978). Effect of human error on the availability of periodically inspected redundant systems. Microelectronics Reliability, 17(3), 351. https://doi.org/10.1016/0026-2714(78)91186-1 [Link]Steinert, Steffen (2023). Anthropology and Value. Interdisciplinary Value Theory, 51-65. https://doi.org/10.1007/978-3-031-10733-7_4 [Link]